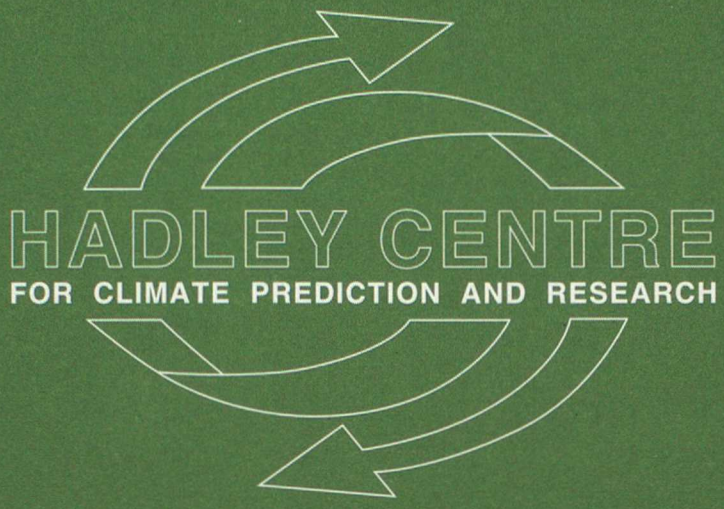

A description of the Second Hadley Centre Coupled Model (HADCM2)

by

T C Johns

CRTN 71

June 1996

CLIMATE
RESEARCH
TECHNICAL
NOTE

Hadley Centre
Meteorological Office
London Road
Bracknell
Berkshire RG12 2SY

CLIMATE RESEARCH TECHNICAL NOTE NO. 71

A DESCRIPTION OF THE SECOND HADLEY CENTRE COUPLED MODEL (HADCM2)

by

T C Johns

Hadley Centre for Climate Prediction and Research
Meteorological Office
London Road
Bracknell
Berkshire RG12 2SY

NOTE: This paper has not been published. Permission to quote from it should be obtained from the Director of the Hadley Centre.

A description of the Second Hadley Centre Coupled Model (HADCM2)

T. C. Johns

Hadley Centre for Climate Prediction and Research, Meteorological Office, London Road, Bracknell, RG12 2SY, UK

21 June 1996

Abstract

This note describes the second major version (known as 'HADCM2') of the Hadley Centre coupled ocean-atmosphere general circulation model (OAGCM), which has been developed for use in studies of climate change. It includes various physical and technical improvements relative to the first-generation coupled model ('UKTR') used at the Hadley Centre. HADCM2 runs under the UKMO Unified Model (UM) system, and is just one of the many possible configuations of the UM. Here, a scientific description of the model formulation is given, quoting the values of parameters used in the associated dynamical and physical parametrizations. Some details are given of known technical problems concerning conservation of mass, water and especially energy in the model components. The importance attached to ensuring exact repeatability of results is also noted. The reader is referred to other scientific and technical UM documentation for full details of the equations used, numerical methods and coding details.

1 INTRODUCTION

Many climate modelling groups worldwide are involved in developing OAGCMs to improve understanding of climate processes, and to perform more realistic time dependent simulations of climate change (for a recent summary see WCRP 1995). This note documents a new OAGCM developed at the Hadley Centre for just such a purpose, building on the experience gained with UKTR, its predecessor, which was used for transient climate change experiments run on the Cyber 205 computer some years ago. As well as running on a much faster supercomputer (Cray C90 currently), and in a completely different software environment (the UKMO Unified Model system or 'UM' - Cullen 1993)), the new model includes enhancements to its formulation and resolution compared with the original coupled model described by Murphy (1995) and Murphy and Mitchell (1995). As in UKTR the oceanic component of the model is based on the Bryan-Cox primitive equation code, but recoded to interface to the UM system. HADCM2's atmospheric component has been completely rewritten. In particular, the atmospheric dynamics scheme is completely different from UKTR, being based on a new grid type. This has led to some knock-on changes in some of the physical parametrizations. The ocean and sea ice components are also modified in significant ways from UKTR as described below.

The model components are now described briefly, followed by some discussion of the conservation properties of the model and repeatability of results. For fuller details of the governing equations and numerical methods used, refer to the relevant documents listed in Appendix A. Appendices B and C give additional details of source code modification sets and code switch settings which were used in the HADCM2 model configuration.

2 RESOLUTION, GRID LAYOUT AND LAND-SEA MASK

The horizontal resolution of the model is 2.5 degrees in latitude (73 rows) by 3.75 degrees in longitude (96 columns), as in UKTR. This gives a grid spacing of 278 km in the North-South direction and 417 km East-West at the equator reducing to 295 km at 45 degrees North and South - comparable to a T42 spectral model resolution. The numerics are such that gridpoints are ordered from west to east, and from north to south in the atmosphere model but south to north in the ocean model. The first gridpoint on the atmospheric mass grid is situated at the North Pole, and (nominally) on the Greenwich meridian.

To simplify coupling between atmosphere and ocean the layout of the horizontal grid and coastline in the ocean model have been chosen exactly congruent to the atmosphere, with the exception that the northern row is considered to be land (a polar island) in the ocean model but sea in the atmospheric model. This is an expedient measure to avoid difficulties in specifying boundary conditions at the coordinate singularity. Conservation of atmospheric fluxes into the ocean is therefore achieved without the need for horizontal interpolation or redistribution. An island representing Iceland, absent in UKTR, is included in the new model. The land-sea mask is shown in Figure 1.

Vertical resolution is enhanced in both components relative to UKTR, from 11 to 19 levels in the atmosphere, and 17 to 20 levels in the ocean. The sea ice component remains a 'zero-layer' model sharing the ocean model horizontal grid, but with the addition of simple ice and snow advection (Bryan 1969b).

3 ATMOSPHERE AND LAND SURFACE MODEL

In keeping with the international guidelines on plug-compatible code interfaces (Kalnay 1989) the UM system allows various choices for the physical code sections in the atmospheric component of the model. The code versions chosen from the system libraries in HADCM2 are listed in Table 1, with a one-line summary of the features of each scheme chosen.

The atmospheric model equations are a quasi-hydrostatic version of the full primitive equations in spherical polar coordinates with a complete representation of the Coriolis force in which the usual shallow atmosphere approximation is relaxed (White and Bromley 1995). Physical

Code Section (number)	Version	Description
SW radiation (1)	2A	Combined downward diffuse beam; 3 cloud layers
LW radiation (2)	1A	Original Slingo and Wilderspin scheme
Boundary layer (3)	2C	Modified rapidly-mixing scheme
Large scale precip (4)	2B	Consistent with downdraughts; fully divergent ice fallout
Convective precip (5)	2A	Updraught and downdraught mass flux scheme
Gravity wave drag (6)	1A	Richardson number dependent/Froude scheme
Vertical diffusion (7)	1A	Standard scheme
Surface hydrology (8)	1A	Single layer scheme
Large scale cloud (9)	1A	Standard scheme; triangular distribution function
Adjustment (10)	1A	Standard scheme
Advection (12)	1A	Standard scheme (not positive-definite)
Diffusion/filtering (13)	1A	Standard scheme

Table 1: Choices of plug-compatible code sections in atmospheric component of HADCM2.

parametrizations and numerical diffusion are represented by 3-dimensional source and sink vector functions of the main state variables. The predicted state variables are surface pressure, horizontal wind components, and two conserved thermodynamic variables "liquid water potential temperature" and "total water mixing ratio" related to potential temperature and specific humidity via the cloud water content (Smith 1990). Dynamical boundary conditions are the orographic height at the lower boundary and the implied mass continuity condition that vertical velocities through the upper and lower coordinate boundary vanish. Various other boundary conditions related to the physical parametrizations (particularly the land surface and hydrology schemes) are imposed via climatological fixed or seasonally-varying datasets. A 30 minute timestep is used to compute increments from both dynamical and physical parameterisations, although full radiation calculations are performed only every 3 hours for economy. In UKTR, a 10 minute timestep was used, except for radiation.

An Arakawa 'B'-grid (Arakawa and Lamb 1977) layout is used for horizontal discretization in the atmospheric model, in place of the Arakawa 'A'-grid used in UKTR, as the revised dynamics scheme achieves better accuracy on this staggered grid. The layout places surface pressure and the thermodynamic variables at the centre of the gridcell with wind components at the corners. A hybrid coordinate (Simmons and Burridge 1981) is used for the vertical discretization rather than the sigma coordinate used in UKTR. The bottom 4 of the 19 layers (Table 2) are terrain-following sigma layers and the top 3 layers pure pressure layers, with a smooth transition in between.

A split-explicit scheme (Cullen and Davies 1991) integrates the equations in time, the geostrophic adjustment process being separated from the advection part. A 10 minute timestep is used for adjustment, iterated three times per 30 minute advection timestep. Averaged velocities over the three adjustment timesteps are used for advection, which is integrated in time using the Heun scheme (Mesinger 1981). The finite difference scheme is 4th-order accurate in space. Geostrophic adjustment is resolved more accurately than in UKTR as a result of the staggered grid layout, and a longer advection (and hence physics) timestep is made possible by the split adjustment and advection parts.

The dynamical equations in their numerical form formally conserve mass, energy, momentum, angular momentum and total water in the absence of source and sink terms. Fourier damping of unstable zonal wavenumbers is necessary at high latitudes, damping weights being recomputed every 6 hours according to local wind strength. The variables filtered are mass-weighted winds during adjustment and after diffusion, and mass-weighted increments to thermodynamic variables from advection. In addition, an iterated del-squared diffusion process is applied globally to mass-weighted liquid water potential temperature and winds (3 iterations except in the top

Layer	A (Pa) layer centre	A (Pa) layer boundary	B layer centre	B layer boundary	Hybrid coordinate
		0.005×10^4		0.000	0.0005
19	0.046×10^4		0.000		0.005
		$0.100\text{x}10^4$		0.000	0.010
18	0.148×10^4		0.000		0.015
		0.200×10^4		0.000	0.020
17	0.296×10^4		0.000		0.030
		0.400×10^4		0.000	0.040
16	0.553×10^4		0.002		0.057
		0.718×10^4		0.003	0.075
15	0.886×10^4		0.011		0.100
		1.065×10^4		0.018	0.125
14	1.180×10^4		0.031		0.149
		1.300×10^4		0.045	0.175
13	1.366×10^4		0.063		0.200
		1.434×10^4		0.082	0.225
12	1.458×10^4		0.104		0.250
		1.482×10^4		0.127	0.275
11	1.469×10^4		0.153		0.300
		1.456×10^4		0.179	0.325
10	1.401×10^4		0.215		0.355
		1.345×10^4		0.251	0.385
9	1.232×10^4		0.299		0.422
		1.118×10^4		0.348	0.460
8	0.947×10^4		0.410		0.505
		0.773×10^4		0.473	0.550
7	0.581×10^4		0.541		0.599
		0.385×10^4		0.611	0.650
6	0.241×10^4		0.675		0.699
		0.094×10^4		0.741	0.750
5	0.047×10^4		0.788		0.793
		0.000×10^4		0.835	0.835
4	0.000×10^4		0.870		0.870
		0.000×10^4		0.905	0.905
3	0.000×10^4		0.930		0.930
		0.000×10^4		0.956	0.956
2	0.000×10^4		0.975		0.975
		0.000×10^4		0.994	0.994
1	0.000×10^4		0.997		0.997
		0.000×10^4		1.000	1.000

Table 2: Distribution of 19 hybrid vertical layers and layer boundaries in atmosphere model. Note: The hybrid coordinate is defined as ($A/10^5$ Pa) + B.

layer which has only one iteration), and mass-weighted total water (2 iterations). See Table 3 for details of the level-dependent diffusion parameters. The e-folding times for 2 and 4 gridlength waves associated with diffusion are 6.9 and 29 hours respectively for total water, and 3.7 and 31 hours respectively for other variables. Both filtering and diffusion introduce an energy loss into the model, which is numerically corrected with a 1-day lag by adding a globally constant temperature increment computed daily as a global heat budget residual taking account of all fluxes into the system. Small losses of mass resulting from numerical rounding are also corrected with a 1-day lag.

Layer	K(u,v,theta)	N(u,v,theta)	K(q)	N(q)	RH threshold
19	4.0×10^{6} m^2 s^{-1}	1	1.2×10^{8} m^2 s^{-1}	2	0.85
18	8.0×10^{8} m^2 s^{-1}	3	1.2×10^{8} m^2 s^{-1}	2	0.85
17	8.0×10^{8} m^2 s^{-1}	3	1.2×10^{8} m^2 s^{-1}	2	0.85
16	8.0×10^{8} m^2 s^{-1}	3	1.2×10^{8} m^2 s^{-1}	2	0.85
15	8.0×10^{8} m^2 s^{-1}	3	1.2×10^{8} m^2 s^{-1}	2	0.85
14	8.0×10^{8} m^2 s^{-1}	3	1.2×10^{8} m^2 s^{-1}	2	0.85
13	8.0×10^{8} m^2 s^{-1}	3	1.2×10^{8} m^2 s^{-1}	2	0.85
12	8.0×10^{8} m^2 s^{-1}	3	1.2×10^{8} m^2 s^{-1}	2	0.85
11	8.0×10^{8} m^2 s^{-1}	3	1.2×10^{8} m^2 s^{-1}	2	0.85
10	8.0×10^{8} m^2 s^{-1}	3	1.2×10^{8} m^2 s^{-1}	2	0.85
9	8.0×10^{8} m^2 s^{-1}	3	1.2×10^{8} m^2 s^{-1}	2	0.85
8	8.0×10^{8} m^2 s^{-1}	3	1.2×10^{8} m^2 s^{-1}	2	0.85
7	8.0×10^{8} m^2 s^{-1}	3	1.2×10^{8} m^2 s^{-1}	2	0.85
6	8.0×10^{8} m^2 s^{-1}	3	1.2×10^{8} m^2 s^{-1}	2	0.85
5	8.0×10^{8} m^2 s^{-1}	3	1.2×10^{8} m^2 s^{-1}	2	0.85
4	8.0×10^{8} m^2 s^{-1}	3	1.2×10^{8} m^2 s^{-1}	2	0.85
3	8.0×10^{8} m^2 s^{-1}	3	1.2×10^{8} m^2 s^{-1}	2	0.85
2	8.0×10^{8} m^2 s^{-1}	3	1.2×10^{8} m^2 s^{-1}	2	0.90
1	8.0×10^{8} m^2 s^{-1}	3	1.2×10^{8} m^2 s^{-1}	2	0.95

Table 3: Values of level-dependent diffusion parameters and relative humidity thresholds for cloud scheme in atmospheric component of HADCM2.

In regions of strong local gradient the advection scheme can produce negative humidity. To correct this, negative values are set to zero and remaining points in the same layer rescaled to preserve the layer total. If there is insufficient positive moisture to allow a redistribution, negative values are reset to zero without rescaling positive values, resulting in a net source of atmospheric moisture. Even in layers which conserve moisture, systematic local sources and sinks will generally be created, but on a large scale this effect is relatively minor, the zonal average absolute flux due to vertically-integrated sources/sinks in the column being below 0.5% of the zonal average absolute net precipitation minus evaporation flux in an annual mean sense at all latitudes apart from the South Pole. This correction scheme is expected to be improved in future to prevent non-conservation.

Gravity wave drag is applied to momentum components in the free atmosphere using a parametrization based on a prescribed sub-grid scale orographic variance field and the vertical stability profile as a function of height through the atmospheric column (Palmer et al. 1986). Anisotropies in the orographic variance are neglected in computing the drag in this scheme.

The radiation scheme consists of two parts; solar calculations, which use four spectral bands as defined in Slingo (1989), and longwave calculations, which use six spectral bands as defined in Slingo and Wilderspin (1986). Both the diurnal cycle and annual cycle of insolation are represented, with the incoming solar part of the radiation rescaled on each physics timestep to give more smoothly varying radiative forcing during daylight hours. Interactive cloud optical

properties are computed from the derived cloud water and ice contents (Slingo 1989) assuming an effective droplet radius of 7 μm for water cloud and 30 μm for ice cloud. Radiative transfer calculations take account of the effects of water vapour, carbon dioxide, and ozone (specified from zonal average monthly climatological data) in addition to clouds. Maximum/random overlap of all cloudy layers is assumed in the longwave, but randomly overlapped low, medium and high cloud is assumed in the solar. Low, medium and high cloud groups are defined as layers 1–5, 6–9 and 10–18 respectively. Within each cloud group, the layer with the greatest fractional cover defines the cloud cover and cloud level for the whole group (taking the lowest level if more than one layer is equal), the cloud water from all layers in the group being assumed to be uniformly distributed over that cloud fraction. Surface albedo at ice-free sea points and for leads is calculated as a specified function of solar zenith angle for the direct beam, ranging from 0.05 at the zenith to 0.06 at 45 degrees and 0.17 at 75 degrees, and 0.06 for the diffuse beam. Over sea ice, albedo varies linearly from 0.80 for surface temperature at and below 263.15 K to 0.50 at 273.15 K. Bare ice and snow-covered ice are not differentiated. Over land, albedo is computed from snow-free and deep snow albedos specified according to vegetation type, based on predicted snow depth and surface temperature. In UKTR, solar radiation was not resolved into separate spectral bands as in the present model, so a fixed fractional split of net solar into penetrating and non-penetrating flux into the ocean was assumed. Now, the ocean penetrating component of radiation is computed as a separate band (250 to 690 nm) in the radiation scheme.

Large-scale cloud water and total cloudiness are computed at each point from the total water variable, according to the local temperature and a reference relative humidity, using a simple functional relation to determine the fraction of total water in cloud form. See Table 3 for details of the relative humidity thresholds for the formation of cloud on each model level. For the purposes of radiation and precipitation, cloud water is split into liquid and ice fractions. The cloud ice fraction increases as a smoothly varying function of temperature from zero to the total amount over the temperature range 0 to -15 degrees C (Smith 1990).

The boundary layer can occupy up to the bottom 5 atmosphere model layers. A first-order turbulent mixing scheme is used to mix the conserved thermodynamic variables and momentum in the vertical (Smith 1990). Over land, surface roughness characteristics are prescribed according to climatological surface type, but at sea points the roughness length over open water is computed from local windspeeds using the Charnock formula (Charnock 1955) with a lower limit of 10^{-4} m in calm conditions. Partial sea ice cover is allowed in surface calculations at ocean points, with separate fluxes computed for sea ice and leads within an icy gridbox. In order to resolve the diurnal cycle of surface temperature over sea ice, a small surface areal heat capacity equivalent to about 5 cm of water is assumed, while the surface ocean temperature within the leads portion of an icy gridbox is assumed fixed at -1.8 degrees C from the atmospheric point of view (though this is not necessarily the case in the ocean model). A 4-layer soil temperature model (Warrilow et al. 1986) is embedded in the land surface part of the scheme. The choice of soil layer thicknesses is designed to resolve both the diurnal and seasonal cycles with minimal distortion. A zero heat flux condition is imposed at the base of the soil model to conserve heat within the system. Fluxes from the boundary layer are computed for coupling with the sea ice and ocean model, the new model taking account of ocean surface currents (neglected in UKTR) as well as lowest level winds in computing exchange coefficients for heat, moisture and momentum fluxes. Accounting for ocean currents is potentially important in determining surface stress in equatorial regions, where surface currents are significant compared with surface winds (Pacanowski 1987).

Surface hydrology calculations take account of storage of water in a vegetative canopy in addition to ground storage. Canopy evaporation and transpiration, throughfall of moisture from the canopy to the ground, and surface and sub-surface runoff are modelled according to local moisture availability, canopy and ground water content and prescribed parameters (fixed throughout the year) for vegetative fraction, canopy capacity, hydraulic conductivity, infiltration rate, wilting point, root depth, stomatal resistance, critical soil moisture limit for evaporation, and Eagleson's exponent (Warrilow et al. 1986). The scheme is similar to that in UKTR

except that in calculating canopy throughfall and surface runoff, a distribution of rainfall rate within each gridbox rather than a uniform value is assumed (Dolman and Gregory 1992). The model also differs from UKTR in that river outflow is now included, giving the possibility of ocean salinity feedbacks via land changes. Surface and sub-surface runoff are converted into river outflow using predefined river catchments over land and associated coastal outflow points defined relative to the model grid, taking account of actual geographical catchments rather than basing them on the slope of the model orography. River transport is not modelled explicitly, so runoff is transported instantaneously to the coast.

Large-scale (dynamic) rainfall and snowfall calculations are based on cloud water and ice contents and are generally similar to those in UKTR (Smith 1990). Evaporation of falling precipitation, enhanced precipitation rates via seeding from layers above, and phase changes between cloud water and ice are represented. The ice fallout scheme has been modified to allow cloud ice to contribute to the water and ice budget of lower levels as it falls, rather than falling instantaneously through to the ground.

Convective rainfall and snowfall are calculated using a mass flux penetrative convection scheme (Gregory and Rowntree 1990), similar to UKTR but with the addition of an explicit downdraught representation (Gregory and Allen 1991). Mixing of convective parcels with environmental air, forced entrainment and detrainment, and evaporation of falling precipitation are all modelled. Convective cloud amounts are computed from the column condensed water path via a simple functional relation (Slingo et al. 1988).

The values of the scalar parameters used in the various dynamical and physical parametrization schemes are summarised in Table 4.

Atmosphere component parameter	Parameter name in code	Value
No of spectral bands (SW)	H_SWBANDS	4
No of spectral bands (LW)	H_LWBANDS	6
Adjustment steps per advection step	A_ADJSTEPS	3
Steps between SW radiation calls	A_SW_RADSTEP	6
Steps between LW radiation calls	A_LW_RADSTEP	6
Steps between convection calls	A_CONV_STEP	1
Steps between energy correction calc	A_ENERGYSTEPS	48
Steps between filter weight calc	A_NSET_FILTER	1
External gravity wave speed	GRAV_WAVE_SPEED	350.0 m s^{-1}
Filtering safety multiplying factor	FILTERING_SAFETY_FACTOR	0.01
Equivalent-CO_2 conc. (control)	CO2START	4.9×10^{-4} kg kg^{-1}
Max albedo of sea ice (cold)	ALPHAC	0.80
Min albedo of sea ice (melting)	ALPHAM	0.50
Cold-to-melting sea ice range	DTICE	10 K
Surface gravity wave constant	KAY_GWAVE	3.8×10^{-5} m^{-1}
Bottom level for gravity wave stress	START_LEVEL_GWDRAG	3
Bottom level for vertical diffusion	BOTTOM_VDIF_LEVEL	10
Top level for vertical diffusion	TOP_VDIF_LEVEL	19
Reference coefficient for vert diff	VERTICAL_DIFFUSION	1.0×10^{-8} $(Nm^{-2})^2$ s^{-1}
Poleward limit for vert diff	LATITUDE_BAND	30.0 degrees
Advection weighting term	NU_BASIC	0.167
Cloud liq water for ppn (sea)	CW_SEA	2.0×10^{-4} kg m^{-3}
Cloud liq water for ppn (land)	CW_LAND	8.0×10^{-4} kg m^{-3}

Table 4: Scalar parameters associated with the dynamical and physical parametrization schemes in the atmospheric component of HADCM2.

4 OCEAN MODEL

The ocean component of the model is based on the Bryan-Cox primitive equation model (Bryan 1969a, Cox 1984). The 20 depth levels in the vertical are listed in Table 5, where the depth listed is that of the middle of each layer. Level spacing is small near the surface in order to resolve the mixed layer, the top layer being 10m thick. Bottom topography is derived from the Scripps 1 degree resolution orography dataset (Gates and Nelson 1973), with single gridpoint inlets and basins removed. A 1 hour timestep is used to integrate the model (ie. 2 hour leapfrog timestep), with a Robert time filter applied to suppress the grid-splitting mode and a forward timestep once a day to allow storage of just one time level at model checkpoints. In UKTR, a 20 minute timestep was used.

Level	Depth (m)	Thickness (m)	Vertical diffusivity (10^{-5} m^2 s^{-1})
1	5.0	10.0	-
2	15.0	10.0	1.03
3	25.0	10.0	1.06
4	35.1	10.2	1.08
5	47.9	15.3	1.11
6	67.0	23.0	1.16
7	95.8	34.5	1.22
8	138.9	51.8	1.32
9	203.7	77.8	1.46
10	301.0	116.8	1.68
11	447.1	175.3	2.01
12	666.3	263.2	2.50
13	995.6	395.3	3.23
14	1501.0	615.0	4.34
15	2116.0	615.0	6.06
16	2731.0	615.0	7.79
17	3347.0	615.0	9.51
18	3962.0	615.0	11.23
19	4577.0	616.0	12.95
20	5193.0	616.0	14.68

Table 5: Vertical levels and background tracer vertical diffusivity between level and level above in the ocean model.

An energy balance mixed layer model based on Kraus and Turner (1967) is embedded in the model, like that used in UKTR. Any negative surface buoyancy flux into the ocean surface is convectively mixed down to a neutrally buoyant level (in terms of potential density relative to the surface). 15% of the gravitational potential energy released by this convection, and 70% of the work done by the wind on the ocean surface, are assumed to be available for turbulent kinetic energy (TKE). The amount of available TKE is assumed to decay exponentially with depth, with an e-folding scale of 100m. Mixing continues down to a level at which the density profile is statically stable and the TKE is depleted. Any subsurface static instability (for example, caused by horizontal advection of light water masses) is effectively removed at the end of the timestep using 5 iterations of the convective mixing algorithm described by Cox (1984). Only potential temperature and salinity are mixed by these schemes.

Further vertical mixing is provided at all depths through vertical diffusion both of tracers (potential temperature and salinity) and momentum. The vertical diffusivity is the sum of a depth-dependent constant background term and a term dependent on Richardson number (Pacanowski and Philander 1981). In practice it is found that the latter term is small everywhere

except in the mixed layer. For momentum, a background value of 1.0×10^{-5} m^2 s^{-1} is used at all levels. The background profile for tracers (Table 5) is a close fit to the theoretical/observational estimate of Kraus (1990), and the near-surface values are in good agreement with recent direct measurements in the upper 1000m of the ocean (Ledwell et al. 1993). UKTR used 1.0×10^{-5} m^2 s^{-1} at all levels (the surface value in the present model), and so had lower tracer diffusivities at all depths.

A horizontal momentum diffusivity (eddy viscosity) of 1.5×10^5 (1+cos(latitude)) m^2 s^{-1} is applied. This latitudinal profile spreads the subtropical western boundary currents in the model sufficiently to allow them to be resolved at the model resolution, while avoiding a restriction on the timestep due to numerical instability in the diffusion equation at high latitudes. The cosine dependence of diffusivity was omitted in UKTR. Tracers are diffused along isopycnal surfaces (Redi 1982), with a depth-dependent diffusivity of (400 + 1600exp(-z/500)) m^2 s^{-1}, where z is the depth in metres. A background horizontal diffusivity of 40 m^2 s^{-1} is also applied to tracers to control gridscale noise.

There is no direct connection between the Mediterranean Sea and Atlantic Ocean with the modelled coastline and bathymetry, but mixing of temperature and salinity across the Straits of Gibraltar is parametrized by completely mixing the easternmost point of the Atlantic with the westernmost point of the Mediterranean having the same depth of water, in the manner of Manabe and Stouffer (1988). Mixing occurs over the top 13 layers, to a depth of 1200m, on the assumption that Mediterranean water will sink to at least this depth after flowing over the sill. Mixing between the Atlantic and Mediterranean was not represented in UKTR.

5 SEA ICE MODEL

The thermodynamics of the model is based on the zero-layer model of Semtner (1976). A parameterisation of ice concentration A based on that of Hibler (1979), is included. A is not allowed to exceed 0.995 in the Arctic and 0.980 in the Antarctic since completely unbroken ice cover is rarely observed in reality even in pack ice. Ice depth can be increased by the formation of "white ice" (Ledley 1985) where the weight of snow forces the ice-snow interface below the water line.

The effect of sea ice formation and melt on ocean salinity is accounted for within the model, assuming a constant salinity of 0.6% for sea ice. Sublimation increases ocean salinity, as the salt is assumed to blow into leads, and white ice formation reduces it to account for the salt added in converting snow to ice. Snowfall reduces ocean salinity in leads, and accumulates onto ice, and all rainfall is assumed to reach the ocean through leads.

Surface fluxes over the ice and leads fractions of each grid box, and surface temperatures, are calculated separately within the atmosphere component of the model, assuming a linear temperature profile in the ice. In UKTR wind mixing (mechanical) energy was not applied under ice, leading to rather shallow mixed layers, so in the present model a windmixing energy, calculated using the drag coefficient appropriate for leads and weighted by the leads fraction of the grid square, is applied to the ocean. Oceanic heat flux into the base of the ice is related to the temperature difference between the ocean top level and the base of the ice (assumed to be at a freezing point of -1.8 degrees C), as in the previous model, with a coupling coefficient of 20 W m^{-2} K^{-1}.

A simple parametrization of sea ice dynamics, omitted in UKTR, is now included, based on Bryan (1969b). Ice thickness, concentration and snow depth are advected using the top layer ocean current, and an upstream advection scheme. Ice rheology is crudely represented by preventing convergence of ice once the ice depth reaches 4m. Del-squared horizontal diffusion of ice depth is also applied, with a coefficient 2000 m^2 s^{-1}.

In UKTR, net heat fluxes from the leads fraction of a grid square with ice were used within the ice model to melt or form ice via Hibler's (1979) leads formulation, rather than to cool or warm the ocean. This gives unrealistic behaviour with dynamics added to the model; as soon as a small amount of ice advected over a warm but cooling ocean, the net heat flux from ocean to

Ocean/Sea ice component parameters	Name in code or symbol	Value
No steps per ocean forward timestep	NMIX	24
Semi-implicit coriolis coefficient	ACOR	0.75
Robert time filtering constant	PNU	0.01
First tracer row filtered	JFRST	6
Tracer row defining zonal scale	JFT0	7
Last tracer row filtered in S.Hem	JFT1	7
First tracer row filtered in N.Hem	JFT2	67
Velocity row defining zonal scale	JFU0	7
Last velocity row filtered in S.Hem	JFU1	7
First velocity row filtered in N.Hem	JFU2	66
Wind mixing energy scaling factor	LAMDA	0.7
Decay scale of WME with depth	DELTA_SI	100.0 m
Convectively generated energy decay	EPSILON	0.15
Background momentum vertical mixing	FNUB_SI	1.0×10^{-5} m^2 s^{-1}
Surface tracer vertical mixing	KAPPA0_SI	1.0×10^{-5} m^2 s^{-1}
Rate of increase with depth	DKAPPA_DZ_SI	2.8×10^{-8} m s^{-1}
Ri-dependent momentum mixing coeff	FNU0_SI	5.5×10^{-3} m^2 s^{-1}
Max stable value of vertical mixing	STABLM_SI	0.01 m^2 s^{-1}
Momentum diffusion lat-dep 'X' coeff	AM0_SI	1.5×10^{5} m^2 s^{-1}
Momentum diffusion lat-dep 'Y' coeff	AM1_SI	1.5×10^{5} m^2 s^{-1}
Isopycnal diffusion surface value	AHI1_SI	2.0×10^{3} m^2 s^{-1}
Isopycnal diffusion bottom value	AHI2_SI	400.0 m^2 s^{-1}
Isopycnal diffusion decay scale	AHI3_SI	500.0 m
Maximum slope allowed	SLOPE_MAX	0.01
Background tracer horiz diffusion	AH_SI	40.0 m^2 s^{-1}
Maximum no of relaxation scans	MXSCAN	100
Over-relaxation coefficient	SOR	1.60
Convergence criterion ratio	CRIT	1.0×10^{-4}
Ocean-ice diffusion coeff in N.Hem	EDDYDIFFN	2.5×10^{-5} m^2 s^{-1}
Ocean-ice diffusion coeff in S.Hem	EDDYDIFFS	2.5×10^{-5} m^2 s^{-1}
Salinity of sea ice	SALICE	0.006
Minimum local sea ice depth	H0	0.5 m
Minimum gridbox mean sea ice depth	HICEMIN	1.0×10^{-4} m
Maximum ice concentration in N.Hem	AMXNORTH	0.995
Maximum ice concentration in S.Hem	AMXSOUTH	0.980
Minimum ice concentration	AICEMIN	0.001
Horiz ice diffusion coefficient	AH_ICE	2.0×10^{3} m^2 s^{-1}
Penetrative solar absorption: band 1	ETA1_SI	1.0 m^{-1}
Penetrative solar absorption: band 2	ETA2_SI	0.059 m^{-1}
Penetrative solar ratio band 1 to 2	RSOL	0.0

Table 6: Scalar parameters associated with the dynamical and physical parametrization schemes in the ocean and sea ice components of HADCM2.

atmosphere tending to cool the ocean was entirely diverted into forming ice instead. Unlike in UKTR, the penetrative part of shortwave radiation into leads is now allowed to warm the ocean as it would at open ocean grid squares, and all other surface heat fluxes into leads are split, so that a fraction of them equal to the ice concentration is used to form/melt ice by the ice model. The remainder is applied to the ocean model.

The values of the scalar parameters used in the various dynamical and physical parametrization schemes in the ocean and sea ice components are summarised in Table 6.

6 COUPLING AND FLUX ADJUSTMENTS

The coupling cycle consists of a one-day integration of the atmosphere model during which fluxes of heat, momentum, water and wind-mixing energy are averaged followed by a one-day integration of the ocean model. In UKTR a longer, 5 day, coupling cycle was used. During the ocean leg, averaged atmospheric fluxes are supplied from the preceding atmosphere leg, with additional fluxes of heat and fresh water ('flux adjustments') calibrated from the spinup phase to keep the ocean surface temperature (SST) and salinity (SSS) close to the specified seasonally-varying reference climatologies.

These flux adjustments are calculated interactively by computing Newtonian relaxation terms proportional to the differences between modelled SST and SSS and their reference climatological values on each timestep, and storing averages over 5 day periods during the spinup. The Newtonian relaxation constant for heat fluxes is 164 W m^{-2} K^{-1}, giving an e-folding timescale of 14.5 days for a 50 m mixed layer, and the relaxation constant for fresh water such that the relaxation timescale for SSS is the same as for SST. Reference climatologies for SST and SSS are taken from monthly mean Levitus (1982) conditions, without any adjustments to SST near sea ice as were made in UKTR. However, in order to strengthen the S. Ocean overturning circulation and improve the bottom water characteristics of the model, following England (1992, 1993) some modifications (generally increasing the surface density) are made to Levitus salinities around Antarctica as outlined in Table 7.

Month	Adjusted Salinity at southern row (75 or 77.5 S) (psu)	Northernmost latitude (row number) for interpolation
May	34.5	72.5 S (row 7)
Jun	34.7	70.0 S (row 8)
Jul	34.9	67.5 S (row 9)
Aug	34.9	67.5 S (row 9)
Sep	34.8	70.0 S (row 8)
Oct	34.6	72.5 S (row 7)

Table 7: Adjustments to Levitus (1982) reference sea surface salinities in the ocean model. Note: The southern row is defined as row 6 (75 S) in the Ross Sea sector, row 5 (77.5 S) elsewhere. Reference salinities are linearly interpolated from the adjusted value at the southern row to the standard Levitus (1982) value at the northern latitude listed. No adjustments are made in other months.

In the climate change experiment, the calibrated flux adjustments (averaged over 25 annual cycles in this study) are applied as prescribed, non-interactive terms. Without them, the coupled model would rapidly drift away from a realistic state. An improvement over UKTR is that flux adjustment of sea ice is no longer required with the inclusion of sea ice dynamics and other changes. Keeping SST close to its reference climatology imposes a strong constraint on the sea ice areal extent, but the sea ice depth is free to adjust to a mutual equilibrium with the

atmosphere and ocean in HADCM2.

7 KNOWN CONSERVATION PROBLEMS

As mentioned in section 3, mass loss due to numerical effects is corrected once a day, based on calculated changes in global mean surface pressure. Despite this correction procedure, a noticeable loss of global mean surface pressure is still present in long runs, of about 1 hPa per century. This is considerably reduced (but not eliminated completely) if 64 bit accuracy is used for this field in dumps, suggesting that the truncation occuring at dumping time (also once a day) is a problem.

The atmospheric component of the model does not conserve total water precisely either, losing about 1 kg m^{-2} $year^{-1}$ relative to the net fluxes of water at the surface. It is not clear what factors contribute to this.

Some ocean-related conservation problems, diagnosed using detailed diagnostics computed over selected periods of the control and anomaly experiments are now summarised.

(i) There are two "intentional" non-conservations: the heat flux adjustment (0.3 W m^{-2} into the ocean on the global average) and the "heat sink" (0.04 W m^{-2}). The latter represents a loss of negative heat when the ocean falls to freezing point right to the bottom and is prevented from getting any colder.

(ii) In the original control and anomaly runs, there is a non-conservation of about 0.015 W m^{-2} (calculated off-line from single-precision fields), in the sense that more heat is being put into the ocean and ice by the surfaces fluxes than appears in the total heat content (ocean temperature and latent heat of ice), when (i) has been taken into account. The heating-rate diagnostics agree with the fluxes rather than the content, so the non-conservation is not arising in the ocean physics. It can be mostly accounted for as a truncation error arising when the ocean temperature fields are written to a dump in 32-bit words with a 24-bit binary mantissa. If this causes the neglect of a proportion $2^{-24} = 6\times10^{-8}$ of the temperature, the volume-average temperature being about 4 K, it happens once a day and the global-average ocean depth is 2500 m, the resulting heat loss is $6\times10^{-8} \times 4 \times 2500 \times 4.2 \times 10^6$ / 86400 = 0.03 W m^{-2} which is of the observed order of magnitude.

(iii) At 2080 the control run was modified so as to write out temperature fields at full precision to the dump. The non-conservation over the period 2180-2200 was 0.0004 W m^{-2} in the opposite sense to (ii) i.e. the ocean is gaining too much heat. The net flux into the ocean over the period is 0.0775 W m^{-2}, so the fractional error is 5×10^{-3}. This can no longer be due to limited precision in the dump, because doubling the length of the mantissa should increase the precision by several orders of magnitude. The largest fluxes involved in computing the net flux are the radiative fluxes, which can be O(100) locally, so 1×10^{-4} is near the limit of single precision for them. This could be a contributory factor to the discrepancy. See also (v).

(iv) The heating-rate diagnostics show that the processes which move heat around within the ocean (advection, diffusion, mixed-layer mixing, convection and Mediterranean outflow) and the filters (Fourier and Robert) all conserve heat to within the accuracy of a single-precision computation $O(1\times10^{-8})$, except for convection. There is a heat loss associated with convection of 0.002 W m^{-2}. This arises from a point in the Persian Gulf which is isolated in the ocean model, and where the salinity has passed the 45 psu value assigned to the "bedrock" beneath the ocean. Convection has set in below the ocean floor, which is at 0 degC, cooling the water above. The problem does not occur in the earlier stages of the runs; presumably the salinity is increasing only slowly. This problem is more serious in unfluxadjusted HADCM2 runs, where the surface salinity is not being corrected. Convection also occurs below the ocean floor at a couple of points in the Red Sea, and the loss of heat is about O(0.1) W m^{-2} by 2100. This was corrected at 2105 in the unfluxadjusted runs by a change to use the ocean number-of-levels array instead of 45 psu to inhibit convection. In HADCM3 (the successor to HADCM2 under development) the convection scheme is different and the number of levels is used.

(v) Considerable effort was invested in checking that the sum of the heating-rate diagnostics

referred to in (iii) equal the change of ocean water heat content. Because of the leapfrog timestep scheme in the ocean, only the even timesteps (0Z-2Z, 2Z-4Z, etc.) are directly relevant to accounting for the change in overall temperature from 0Z to 0Z. The state after odd timesteps influences the evolution only through the Robert filter. It turns out that many of the heating-rate terms, particularly the mixed layer, have a strong "diurnal" cycle, even though there is no such cycle in the atmosphere forcing. Because of this, a mean of the heating-rates over all timesteps does not accurately balance the change in temperature from 0Z to 0Z. It is necessary to obtain mean heating-rates over even timesteps only, except that probably the Robert filter should be taken over odd timesteps only. In the volume average, the sum of the heating-rates and the change in ocean water content match to $O(1\times10^{-5})$ W m^{-2}, which is on the limit of numerical precision because some of the heating-rate terms are O(10). The difficulty of timesteps will be relevant to the reconciliation of the ocean state with any ocean fluxes or rates. The ocean heat sink is such a quantity, which probably should be meaned over even timesteps only in order to be compared with the heat content. This could be relevant to (ii). Since the ice model does not use a leapfrog timestep, there is the possibility of non-conservation in the exchange of heat between ocean water and ice, also possibly involved in (ii).

(vi) There is probably a non-conservation arising from the inconsistent treatment in the atmosphere and ocean models of the row at the North Pole, which is taken as sea in the atmosphere and ice models, and land in the ocean model. This probably means that heat fluxes which should be applied to the ocean model (solar through leads, a proportion of other leads heat fluxes and latent heat of snow falling through the leads) are being lost at this row. Unfortunately fields are not available to compute this loss from HADCM2, which is a non-conservation of the coupled system rather than the ocean submodel alone.

8 REPEATABILITY OF RESULTS

The UM control system has been carefully designed and checked to ensure that results are exactly repeatable at the bit level under a number of possible circumstances which may arise during the long climate integrations. These are:

(i) Stopping and restarting the run at any daily checkpoint, compared with not stopping;

(ii) Restarting after a computer system crash from saved checkpoint dumps;

(iii) Rerunning from saved checkpoint dumps at a later date using the same executable file (possibly with different output diagnostics);

(iv) Running or rerunning multi-tasked on a different number of CPUs (one or more) using the same executable file.

Note that the flexibility of the diagnostic control system ('STASH') in the UM allows HADCM2 to be run with diagnostics selected dynamically, so that different diagnostic sets can be calculated and output in principle with the same executable file (see (iii) above) provided the diagnostics are programmed into the compiled code in the first place.

Efforts have also been made to ensure that repeatability of results is maintained across new releases of the UM system and across changes in the C90 operating system environment. This has been achieved to some extent, but some UM and external system changes imply that repeatability is lost on recompilation, so executable files have been saved from the key integrations performed with HADCM2 to ensure exact reruns are possible. However, repeatability of old runs will defintely not be possible when the C90 is replaced by a different computer.

9 SUMMARY

Table 8 briefly summarises the main differences between UKTR and HADCM2.

Aspect	UKTR	HADCM2
Resolution (atmosphere)	96x72 L11 (A-grid, sigma coord)	96x73 L19 (B-grid, hybrid)
Resolution (ocean)	Congruent, 17 depth levels	Congruent, 20 depth levels
Timestep (atmosphere)	10 minutes	30 minutes
Timestep (ocean)	20 minutes	60 minutes
Coupling cycle	5 days	1 day
Atmospheric dynamics	Centred explicit, leapfrog	Split-explicit, Heun
Solar radiation scheme	Single spectral band	Multiple spectral bands
Cloud radiative properties	Prescribed for given cloud type	Computed interactively
Atmospheric convection	Ignores downdraughts	Includes downdraughts
Boundary layer fluxes	No account of ocean currents	Ocean currents used
Surface hydrology	Assumes homogeneous rainfall	Uses gridbox distribution
River runoff	Not included	Included
Ocean diffusivity	Constant with latitude	1+cos(latitude) function
Vertical tracer mixing	Uniform with depth	Increasing with depth
Mediterranean mixing	Not included	Included
Sea ice dynamics	Not included	Included
Leads fluxes at ice pts	Applied solely to ice budget	Split between ice/ocean
Fields flux adjusted	Ocean SST,SSS and sea ice mass	Ocean SST and SSS only
Reference SST's	Levitus, modified at seaice	Levitus, unmodified
Reference SSS's	Levitus, unmodified	Levitus, modified
Averaging of adjustments	5-day means, 10 year average	5-day means, 25 year average

Table 8: Summary of the main scientific differences between UKTR and HADCM2.

Acknowledgements

The development work for the model was carried out with supplementary support from the Commission of the European Communities (contract EV5V-CT92-0123). This report is largely a reworking of a paper prepared jointly with Ruth Carnell, Jenny Crossley, Jonathan Gregory, John Mitchell, Cath Senior, Simon Tett and Richard Wood, whose help is much appreciated. The calculations of mass, water and energy non-conservation were performed by Jonathan Gregory Simon Tett and Ann Keen. Many other colleagues have helped in the development of the coupled model and the Unified Model software systems described here.

References

Arakawa A, Lamb VR (1977) Computational design of the basic dynamical processes of the UCLA general circulation model. Methods of Computational Physics 17: 174-265, Academic Press.

Bryan K (1969a) A numerical model for the study of the circulation of the world ocean. J Comput Phys 3: 347-376

Bryan K (1969b) Climate and the ocean circulation. III The ocean model. Mon Wea Rev 97: 806-827

Charnock H (1955) Wind stress on a water surface. Quart J Roy Meteor Soc 81: 639

Cox MD (1984) A primitive equation, three dimensional model of the ocean. GFDL ocean group technical report no.1, Princeton NJ, USA, 143 pp

Cullen MJP (1993) The unified forecast/climate model. Meteor Mag 122: 81-94

Cullen MJP, Davies T (1991) A conservative split explicit integration scheme with fourth order horizontal advection. Quart J Roy Meteor Soc 117: 993-1002

Dolman AJ, Gregory D (1992) The parametrization of rainfall interception in GCMs. Quart J Roy Meteor Soc 118: 455-467

England MW (1992) On the formation of Antarctic Intermediate and Bottom Water in ocean general circulation models. J Phys Oceanogr 22: 918-926

England MW (1993) Representing the global-scale water masses in ocean general circulation models. J Phys Oceanogr 23: 1523-1552

Gates WL, Nelson RB (1973) A new tabulation of the Scripps topography on a 1 degree global grid. Part II: Ocean depths. Santa Monica, California, Rand Corp. Contract no. DAHC15-73-0181.

Gregory D, Allen S (1991) The effect of convective scale downdraughts upon NWP and climate simulations. 9th conference on numerical weather prediction, Denver, CO, Amer Meteor Soc: 122-123

Gregory D, Rowntree PR (1990) A mass flux convection scheme with representation of ensemble characteristics and stability dependent closure. Mon Wea Rev 118: 1483-1506

Hibler WD (1979) A dynamic-thermodynamic sea ice model. J Phys Oceanogr 9: 815-846

Kalnay E (1989) Rules for interchange of physical parameterizations. Bull Amer Meteor Soc 70: 620-621

Kraus EB (1990) Diapycnal Mixing. In: Climate-Ocean Interaction, ed. M.E.Schlesinger, Kluwer, Amsterdam, Netherlands, pp 269-293

Kraus EB, Turner JS (1967) A one dimensional model of the seasonal thermocline. Part II. Tellus 19: 98-105

Ledley TS (1985) Sea ice: Multiyear cycles and white ice. J Geophys Res 90: 5676-5686

Ledwell JR, Watson AJ, Law CS (1993) Evidence for slow mixing across the pycnocline from an open-ocean tracer release experiment. Nature 364: 701-703

Levitus S (1982) Climatological Atlas of the World Ocean. NOAA Professional Paper 13, National Oceanic and Atmospheric Administration, Rockville, MD, USA, 173 pp

Manabe S, Stouffer R (1988) Two Stable Equilibria of a Coupled Ocean-Atmosphere Model. J Climate 1: 841-866

Mesinger F (1981) Horizontal advection schemes on a staggered grid, an enstrophy and energy conserving model. Mon Wea Rev 109: 467-478

Murphy JM (1995) Transient Response of the Hadley Centre Coupled Ocean-Atmosphere Model to Increasing Carbon Dioxide. Part I: Control Climate and Flux Adjustment. J Climate 8: 36-56

Murphy JM, Mitchell JFB (1995) Transient Response of the Hadley Centre Coupled Ocean-Atmosphere Model to Increasing Carbon Dioxide. Part II: Spatial and Temporal Structure of Response. J Climate 8: 57-80

Pacanowski RC (1987) Effect of Equatorial Currents on Surface Stress. J Phys Oceanogr 17: 833-838

Pacanowski RC, Philander G (1981) Parameterisation of vertical mixing in numerical models of the tropical oceans. J Phys Oceanogr 11: 1443-1451

Palmer TN, Shutts GJ, Swinbank R (1986) Alleviation of a systematic westerly bias in general circulation and numerical weather prediction models through an orographic gravity wave drag parametrization. Quart J Roy Meteor Soc 112: 1001-1039

Redi MH (1982) Oceanic isopycnal mixing by coordinate rotation. J Phys Oceanogr 12: 1154-1158

Semtner AJ (1976) A model for the thermodynamic growth of sea ice in numerical investigations of climate. J Phys Oceanogr 6: 379-389

Simmons AJ, Burridge DM (1981) An energy and angular-momentum conserving finite-difference scheme and hybrid coordinates. Mon Weather Rev 109: 758-766

Slingo A (1989) A GCM parametrization for the shortwave radiative properties of water clouds. J Atmos Sci 46: 1419-1427

Slingo A, Wilderspin RC (1986) Development of a revised longwave radiation scheme for an atmospheric general circulation model. Quart J Roy Meteor Soc 112: 371-386

Slingo A, Wilderspin RC, Smith RNB (1988) The effect of improved parametrizations on simulations of cloudiness and the earth's radiation budget in the tropics. J Geophys Res 94: 2281-2301

Smith RNB (1990) A scheme for predicting layer clouds and their water content in a general circulation model. Quart J Roy Meteor Soc 116: 435-460

Warrilow DA, Sangster AB, Slingo A (1986) Modelling of land surface processes and their influence on European climate. Met O 20 Dynamical Climatology Technical Note 38, Meteorological Office, Bracknell, UK.

WCRP (1995) Proceedings of the workshop on Global Coupled General Circulation Models (Scripps Institution of Oceanography, La Jolla, California, USA, 10-12 October 1994), WMO/TD-No. 655, 51 pp

White AA, Bromley, RA (1995) Dynamically consistent, quasi-hydrostatic equations for global models with a complete representation of the Coriolis force. Quart J Roy Meteor Soc 121: 399-418

Appendix A - UM scientific/technical documentation papers

The following UM documentation papers contain fuller details of the model equations and parametrization schemes used in HADCM2. Since the model is continually evolving, copies of these documentation papers current to the HADCM2 version have been archived for reference. Copies are available on request from the author at the Hadley Centre, UK Met Office, London Road, Bracknell, Berkshire, RG12 2SY, UK; email: tcjohns@meto.gov.uk.

UM Paper No	Title
P0	Atmospheric model structure
10	Conservative finite difference schemes for a unified forecast/climate model
21	Vertical diffusion
23	Radiation
24	Subsurface, surface and boundary layer processes
25	Canopy, surface and soil hydrology
26	Large-scale recipitation
27	Convection scheme
70	Specification of ancillary fields
40	The ocean model
41.1	Mixed layer formulation
42.1	Penetrative solar radiation
45	The thermodynamic/dynamic sea ice model
47	Tracer transport diagnostics
50	Application of surface heat and fresh water fluxes
51	Isopycnal diffusion scheme
57	Knudsen code for density coefficients

Appendix B - Source code modifications relative to UM 3.2

The following table lists the modification sets applied to the standard source code at UM3.2 in the HADCM2 model, together with a one line summary of their effects. Many of these modifications affect control aspects only, or provide additional potential diagnostic output. Those with a scientific effect are marked **.

Modification set name / *IDENT	Summary
"MEF1.BALIB.FROZEN(CBQM#C)"	Contains ...
IDENT TJNOWRIT	Suppress WRITDUMP printout
IDENT TJ170993	STASH corrections for mass weights, etc.
IDENT SI061093	Correction to MEAD diagnostic code
IDENT HEATSNKZ	Diagnose heat sink at ocean floor
IDENT TJ230793	Fix coupled model repeatability bug
IDENT TJAABW5 **	Modify Antarctic winter ref salinity in spinup
IDENT TJECOR32	Diagnose atmospheric energy correction
IDENT TJWINDSP	Diagnose 10m windspeed
IDENT TJPPN	Diagnose total rain, snow and total ppn
IDENT CH080993 **	Change seaice albedos in atmos
IDENT KAPPAZ32 **	Ocean vertically varying background diffusivity
IDENT SCLMD31E	Top level control logic for SLAB model
IDENT TJSTSHFX	STASH fix for staggered C-grid types
IDENT JT260194	Catch old/PP real MDIs in O2A coupling
IDENT KNUDSEN **	Input KNUDSEN coeffs - override UNESCO
IDENT MEDOUT32 **	Code for mediterranean outflow
IDENT ICYWME32 **	Ocean code to put WME thro leads fract
IDENT JTNOHANY **	Ocean code to suppress HANEY at seaice
IDENT JT101193	Rename old miscellaneous flux ptrs
IDENT JT161193 **	Incorporate dynamic seaice model
IDENT JT301193 **	Seaice/leads advection+diffusion code
DECKS (several) **	Seaice interpolation service routines
IDENT JTEDY025 **	Ocean code to set ocean-ice diffusion
IDENT JG130993	Ocean diagnostic HTN zeroed if not ice
IDENT JG220993 **	Ocean code to zero ice anom flux/FC
IDENT JT040194 **	Ocean code to reapportion HTN at icept
IDENT JG170893	Ocean heating rate/acceleration diags
IDENT MC130993	Fixes to INITHDR1
IDENT TJ300394	STASH and other overwriting hazard bugfixes
IDENT TJSTEP48	Only write TIMESTEPnnn every 48th steps
IDENT TJNOTRAP	Dont trap IO error on PPfile already archived
IDENT JTICEBUD **	Fix ocean-ice budget errors and add diags
IDENT DG020893 **	Fix to detrain, prevents warm climate blowups
"MEF1.BALIB.FROZEN(TJCO2MO1)"	[For CO2-only scenario runs] Contains ...
IDENT TJCO2MOD **	Provide equiv-CO2 scenario via namelist
"MEF1.BALIB.FROZEN(TJSULPH2)"	[For CO2+SO4 scenario runs] Contains ...
IDENT TJSULPH2 **	SO4 direct-effect and provide CO2+SO4 scenarios
"MEF1.BALIB.FROZEN(TJQTSRCE)"	Contains ...
IDENT TJQTSRCE	Output QT source-sink diagnostic on levels
"MEF1.BALIB.FROZEN(JGSALBU2)"	Contains ...
IDENT JG050894	Output salinity budget diagnostics
"MEF1.BALIB.FROZEN(EXPPHDR2)"	Contains ...
IDENT EX100894	Encode JOBID in PP header and other changes
"MEF1.BALIB.FROZEN(GH120795)"	Contains ...
IDENT GH120795	Ensure job resubmission at end of month
"MEF1.SA.UMODEL(JG150895)"	Contains ...
IDENT JG150895	Rescale ocean diags to avoid packing error

Appendix C - Source code *DEF switches used in HADCM2

For completeness, the following list gives other *DEF source code switches which were switched on in HADCM2.

CAL360,CRAY,REPROD
ATMOS,LINEARTS,ABCALC5,FROUDE,EMCORR,GLOBAL
OCEAN,OICECOUP,OFILTER,OISLANDS,OCYCLIC
OSOLAR,OMIXLAY,OIMPDIF,ORICHARD,OISOPYC,OLATVISC,OCHEQUB,OHMEAD
SEAICE,ICEDRIFT
FLUXCORR,RIVERS
ANCILA,ANCILO

FIGURES

Figure 1. Land-sea mask used in HADCM2.

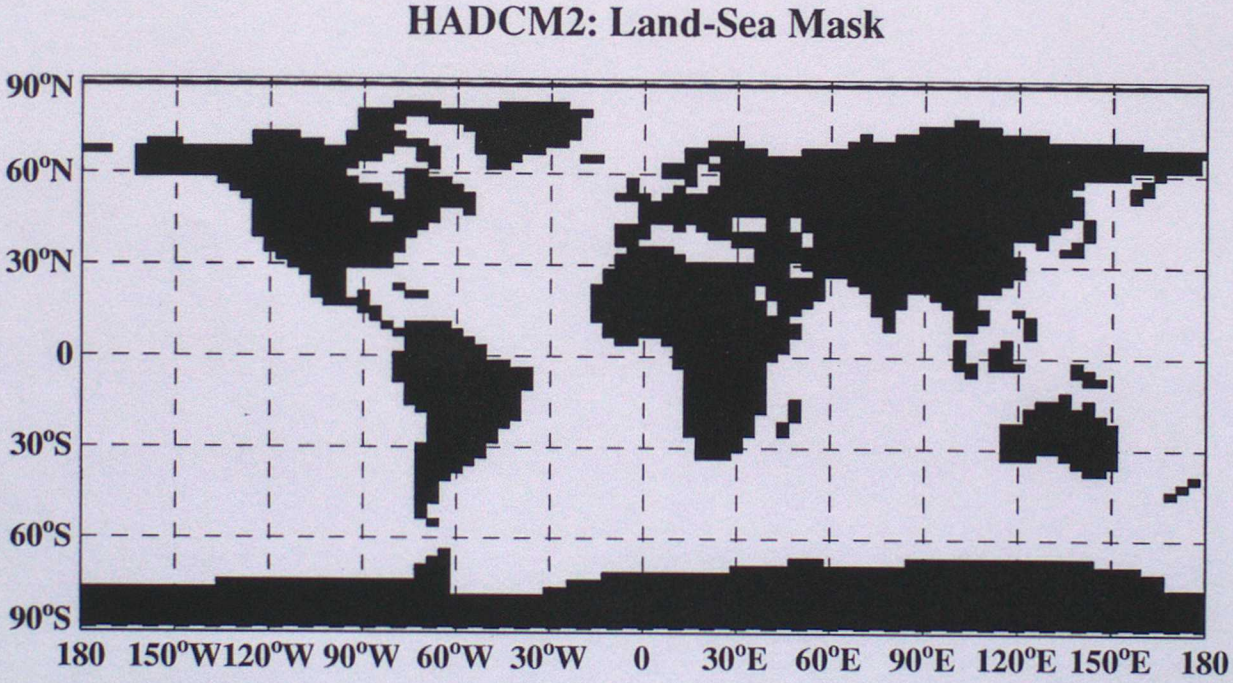

CLIMATE RESEARCH TECHNICAL NOTES

CRTN 1	Oct 1990	Estimates of the sensitivity of climate to vegetation changes using the Penman-Monteith equation. P R Rowntree
CRTN 2	Oct 1990	An ocean general circulation model of the Indian Ocean for hindcasting studies. D J Carrington
CRTN 3	Oct 1990	Simulation of the tropical diurnal cycle in a climate model. D P Rowell
CRTN 4	Oct 1990	Low frequency variability of the oceans. C K Folland, A Colman, D E Parker and A Bevan
CRTN 5	Dec 1990	A comparison of 11-level General Circulation Model Simulations with observations in the East Sahel. K Maskell
CRTN 6	Dec 1990	Climate Change Prediction. J F B Mitchell and Qing-cun Zeng
CRTN 7	Jan 1991	Deforestation of Amazonia - modelling the effects of albedo change. M F Mylne and P R Rowntree
CRTN 8	Jan 1991	The role of observations in climate prediction and research. D J Carson
CRTN 9	Mar 1991	The greenhouse effect and its likely consequences for climate change. D J Carson
CRTN 10	Apr 1991	Use of wind stresses from operational N.W.P. models to force an O.G.C.M. of the Indian Ocean. D J Carrington
CRTN 11	Jun 1991	A new daily Central England Temperature series, 1772-1991. D E Parker, T P Legg and C K Folland
CRTN 12	Jul 1991	Causes and predictability of Sahel rainfall variability. D P Rowell, C K Folland, K Maskell, J A Owen, M N Ward

CLIMATE RESEARCH TECHNICAL NOTES

CRTN 13	Jul 1991	Modelling changes in climate due to enhanced CO2, the role of atmospheric dynamics, cloud and moisture. C A Senior, J F B Mitchell, H Le Treut and Z-X Li
CRTN 14	Sep 1991	Sea temperature bucket models used to correct historical SST data in the Meteorological Office. C K Folland
CRTN 15	Aug 1991	Modelling climate change, and some potential effects on agriculture in the U.K. P R Rowntree, B A Callander and J Cochrane
CRTN 16	Aug 1991	The Boreal Forests and Climate G Thomas and P R Rowntree
CRTN 17	Aug 1991	Development of a Stratosphere-Troposphere Data Assimilation System. R Swinbank.
CRTN 18	Sep 1991	A study of asynchronous coupling using a simple climate model. M K Davey.
CRTN 19	Sep 1991	The Oceanic Carbon Cycle. N K Taylor
CRTN 20	Nov 1991	Worldwide ocean-atmosphere surface fields in Sahel wet and dry years using provisionally corrected surface wind data. M N Ward
CRTN 21	Dec 1991	Coupled tropical ocean global atmosphere models at the UKMO. M K Davey, C Gordon, S Ineson and S Lawrence
CRTN 22	Dec 1991	Empirical parameterisation of tropical ocean-atmosphere coupling. M Allen, M K Davey, D L T Anderson and P D Killworth
CRTN 23	Feb 1992	The temporal evolution of Equatorial Currents in the Indian Ocean D L T Anderson, D J Carrington, R A Corry and C Gordon
CRTN 24	Feb 1992	Stratospheric analyses provided by the U.K. Meteorological Office M J Bailey, A O'Neill and V D Pope

CLIMATE RESEARCH TECHNICAL NOTES

CRTN 25	Feb 1992	Modelling interannual variability in the Indian Ocean using momentum fluxes from the UKMO and ECMWF operational weather analyses. D L T Anderson and D J Carrington
CRTN 26	Mar 1992	A GCM simulation of the impact of Amazonian deforestation on climate using an improved canopy representation J Lean and P R Rowntree
CRTN 27	Mar 1992	The parameterization of rainfall interception in GCMs A J Dolman and D Gregory
CRTN 28	Jun 1992	Development of worldwide marine data eigenvectors since 1985 A W Colman
CRTN 29	Jun 1992	A tropical ocean model with reduced physics M K Davey
CRTN 30	Jun 1992	International Temperature Workshop, Boulder, Colorado, USA, 16 January 1992 Edited by D E Parker
CRTN 31	Jul 1992	Simulation of clear-sky outgoing longwave radiation over the oceans using operational analyses A Slingo and M J Webb
CRTN 32	Sep 1992	A prediction of the transient response of climate J M Murphy
CRTN 33	Nov 1992	LEPS scores for assessing climate model simulations and long-range forecasts. C K Folland
CRTN 34	Jan 1993	Stratospheric Data Assimilation System Guide Editer: R Swinbank
CRTN 35	Mar 1993	A Stratosphere-Troposphere Data Assimilation System R Swinbank and A O'Neill
CRTN 36	Mar 1993	Validation of hydrological schemes for climate models against catchment data. P R Rowntree and J Lean

CLIMATE RESEARCH TECHNICAL NOTES

CRTN 37	Apr 1993	Modelling of palaeoclimates: Examples from the recent past J F B Mitchell
CRTN 38	May 1993	A simulation of seasonality in ENSO forecast skill M K Davey, D L T Anderson and S Lawrence
CRTN 39	Jul 1993	ENSO Prediction experiments using a simple ocean-atmosphere model D-H Wu, D L T Anderson and M K Davey
CRTN 40	Sep 1993	Diagnosis of dynamic sea-surface and sea-level changes from the Cox ocean model J M Gregory
CRTN 41	Sep 1993	Seasonal variations of the clear-sky greenhouse effect: the role of changes in atmospheric temperatures and humidities M J Webb, A Slingo and G L Stephens
CRTN 42	Nov 1993	Sea-level changes under increasing atmospheric CO_2 in a transient coupled ocean-atmosphere GCM experiment. J M Gregory
CRTN 43	Dec 1993	Global and regional patterns of climate change: recent predictions for the Arctic P R Rowntree
CRTN 44	Feb 1994	The effect of changing horizontal diffusion in the atmospheric version of the unified climate model C D Hall and R A Stratton
CRTN 45	Mar 1994	Simulation of El-Niño/Southern Oscillation like variability in a global AOGCM and its response to CO_2 increase. S F B Tett
CRTN 46	Apr 1994	Global data required for monitoring climate change. D E Parker and C K Folland
CRTN 47	May 1994	Seasonal uptake of anthropogenic CO_2 in an ocean general circulation model. N K Taylor

CLIMATE RESEARCH TECHNICAL NOTES

CRTN 48	Jun 1994	A tropic-wide oscillation of boreal summer rainfall and patterns of sea-surface temperature. M N Ward, K Maskell, C K Folland, D P Rowell and R Washington
CRTN 49	Jun 1994	Simulation of the tropical Pacific using a simplified ocean model M A Balmaseda, D L T Anderson and M K Davey
CRTN 50	Sep 1994	Simulation of global mean temperature using a box-diffusion climate model P R Rowntree
CRTN 51	Sep 1994	Seasonal dependence of ENSO prediction skill M A Balmaseda, M K Davey and D L T Anderson
CRTN 52	Nov 1994	Simulation of the Indian Monsoon and Tropical Intraseasonal Variability by a General Circulation Model P M Inness and D Gregory
CRTN 53	Mar 1995	A comparison of modelled surface fluxes with climatological estimates. C Gordon and D K Wright
CRTN 54	Mar 1995	The representation of moist convection in atmospheric models. D Gregory
CRTN 55	Mar 1995	A consistent treatment of the evaporation of rain and snow for use in large-scale models D Gregory
CRTN 56	Apr 1995	Workshop on simulations of the Climate of the Twentieth Century using GISST, 28-30 November 1994, Hadley Centre, Bracknell, UK Edited by C K Folland and D P Rowell
CRTN 57	May 1995	Enhanced shortwave cloud radiative forcing due to anthropogenic aerosols. S E Swartz and A Slingo
CRTN 58	May 1995	The simulation of the tropical oceans in models of different horizontal resolution. C Gordon, D K Wright and C M Roberts
CRTN 59	Sep 1995	The water budget of middle latitude continental regions - a modelling and observational study P R Rowntree
CRTN 60	Sep 1995	Intraseasonal variability of the Indian summer monsoon simulated by the Hadley Centre climate model K Ashok, D Gregory and P M Inness

CLIMATE RESEARCH TECHNICAL NOTES

CRTN 61	Sep 1995	Climate simulations with the Unified Model: AMIP runs C D Hall, R A Stratton and M L Gallani
CRTN 62	Nov 1995	Validation of surface parameters over the oceans in climate simulations with the unified model. C D Hall
CRTN 63	Dec 1995	The GISST2.2 sea surface temperature and sea-ice climatology D E Parker, M Jackson and E B Horton
CRTN 64	Dec 1995	Parametrization of momentum transport by convection. II: Tests in single column and general circulation models. D Gregory, R Kershaw and P M Inness
CRTN 65	Jan 1996	Understanding the sensitivity of a GCM simulation of Amazonian deforestation to the specification of vegetation and soil characteristics. J Lean and P R Rowntree
CRTN 66	Jan 1996	On the efficient calculation of infra-red fluxes and cooling rates using the two-stream equations. J M Edwards
CRTN 67	Jan 1996	The second Hadley Centre coupled ocean-atmosphere GCM: Model description, spinup and validation. TC Johns,RE Carnell,JF Crossley,JM Gregory, JFB Mitchell,CA Senior,SFB Tett and RA Wood
CRTN 68	Feb 1996	The sensitivity of climate simulations to the specification of mixed phase clouds D Gregory and D Morris
CRTN 69	Apr 1996	Using an ensemble of Multi-Decadal GCM simulations ro assess potential seasonal predictability D P Rowell
CRTN 70	May 1996	North Atlantic and European Seasonal Predictability using an Ensemble of Multi-Decadal AGCM Simulations J R Davies, D P Rowell and C K Folland
CRTN 71	Jun 1996	A description of the Second Hadley Centre Coupled Model (HADCM2) T C Johns